Supporting Information:

Bright colloidal gallium-doped $CuInS_2$ quantum dots for luminescent solar concentrators

Haoran Chen,[a] Zhipeng Xu,[a] Zhijun Shi,[a] Fenghuan Zhao,[b] Lixin Cao,[a] Bohua Dong[a] and Chenghui Xia*[a]*

a. School of Materials Science and Engineering, Ocean University of China, No. 1299, Sansha Road, West Coast New District, Qingdao, 266404, PR China

b. Department of Mechanical and Electrical Engineering, Rizhao Polytechnic, 16 Yantai North Road, Rizhao City, Shandong Province, PR China

Corresponding author Email: dongbohua@ouc.edu.cn; c.xia@ouc.edu.cn

Methods

Materials. Copper (I) iodide (CuI, 98%), anhydrous indium acetate [$In(Ac)_3$, 99.99%], anhydrous gallium (III) chloride ($GaCl_3$, 99.99%), 1-dodecanethiol (DDT, 98%), trioctylphosphine (TOP, 90%), diphenylphosphine (DPP, 95%), 1-octadecene (ODE, 90%), oleic acid (OA, 90%), zinc iodide (ZnI_2, 99.99%), zinc stearate [$Zn(St)_2$, Zn 10-12%, 325 mesh], methyl methacrylate (MMA, 99%), poly (methyl methacrylate) (PMMA, high flow type injection stage), azobisisobutyronitrile (AIBN, 98%), tetrahydrofuran (THF, 99%), anhydrous cyclohexane, toluene, methanol and butanol, were purchased from Aladdin®. ODE and OA were separately degassed at 120 °C under vacuum overnight prior to synthesis.

Synthesis of CIS NCs. In a three-necked flask, CuI (0.1 mmol, 0.019 g), $In(Ac)_3$ (0.1 mmol, 0.029 g) and 10 mL of DDT were mixed and degassed under vacuum at 80 °C for 1 hour. The turbid solution was heated to 215 °C under N_2 and kept for 40 min. At the end of the reaction, it was not washed and stored in a glove box filled with N_2.

Cation Exchange to Form CIGS QDs. In a N_2-filled glove box, $GaCl_3$ (1 mmol, 0.176 g) was added to DPP (1 mmol, 0.174 mL) and then heated with constant stirring to 50 °C. After a few minutes, an opaque white viscous liquid was formed, and 0.174 mL of toluene was added to form the $GaCl_3$-DPP precursor. Added 0.1 mmol of CIS to 5 mL of ODE and heated to 120°C at N_2, inject 35 μL of the above $GaCl_3$-DPP precursor at this temperature and react for 1 hour.

Synthesis of CIGS/ZnS QDs. The CIGS QDs solution from the previous step and 5 mL of ODE were filled into a 100 mL three-necked flask and then degassed at 120 °C for 1 hour. The solution was then maintained at 120 °C under N_2 flow. In the meantime, a Zn solution made of ZnI_2 (0.3 mmol, 0.096g) in 1 mL of TOP and 4 mL of ODE was swiftly injected into the CIGS solution. After injection, the temperature was elevated to 200 °C and kept at this temperature for 90 min before being cooled down to 120 °C. The solution is degassed again for 30 minutes and then heated to 220 °C under N_2. Once the temperature stabilized at 220 °C, a ZnS stock solution, prepared by dissolving 2 mmol of $Zn(St)_2$ in 5 mL of OA, 5 mL of DDT and 10 mL of ODE, was slowly injected into the flask at a rate of 1 mL/h for 10 h using a syringe pump. Subsequently, NCs were precipitated with an equal volume of a mixture of methanol and butanol, centrifuged and the supernatant removed, and after three repetitions, dispersed in 5 mL of anhydrous toluene.

Fabrication of LSC Devices. 20 mL of MMA and 2.62 g of PMMA were added to a three-necked flask and degassed for 30 min at room temperature, then the temperature was slowly raised to 80 °C with constant stirring to completely dissolve the PMMA particles to form a mixture, which was subsequently lowered to 45 °C. 0.05 g of AIBN was dissolved in 5 mL of MMA, and then the initiator was added to the mixture and reacted at 50°C for 4h to form a prepolymer with glycerol-like viscosity. The CIGS/ZnS QDs were dried and dispersed in 3 mL of THF. The homogeneously dispersed quantum dot solution was then slowly added to the prepolymer, stirred for 20 minutes, and slowly degassed at room temperature until no bubbles were produced. A clean silicone mat was placed in the middle of the two glass plates, and three sides of the glass plates were clamped with long-tailed clamps to make the silicone mat and the

glass plates fit tightly together to prevent the pre-polymer from overflowing, while the remaining side of the glass plates was used for injection molding. The prepolymer containing CIGS/ZnS QDs was slowly injected into the mold using a syringe. The injection molded glass plate device was placed vertically into an oven at 50 °C to allow the polymerization reaction at a lower temperature for 10 h. At the end of the low-temperature reaction, the polymer turned into a soft solid, and the temperature was continued to be raised to 70 ℃, and the high-temperature polymerization was carried out for 2 h to fully react the residual monomers, and then cooled to room temperature. Finally, the product was cut and polished to 5 × 5 × 0.5 cm to obtain LSC devices. MMA has a strong irritating odor, so the whole experimental procedure was carried out in a fume hood.

Characterizations. Samples for measurement of absorption and PL spectra were prepared by dispersing the CIGS/ZnS QDs product into 3 mL of cyclohexane in a quartz cuvette. The absorption and PL spectra were acquired on a Metash UV-8000 spectrophotometer and Edinburgh FLS 980 spectrophotometer, respectively. The PL quantum yields (PLQYs) were measured on an Edinburgh FLS 1000 fluorescence spectrometer equipped with integrating sphere (see details in supporting method 2). Powder X-ray diffraction patterns were acquired on Bruker D8 Advance X-ray diffractometer equipped with a Cu Kα X-ray source at 1.5406 Å. Inductive coupled plasma-optical emission spectrometry (ICP-OES) measurements were conducted on an Agilent Technologies 5110 ICP-OES instrument equipped with a dichroic spectral combiner and the VistaChip II CDD detector. Samples were prepared by digesting dried products in concentrated HNO_3 (69.5%) and further diluted by 1000 times to reach ppm ranges using 5% HNO_3. X-ray photoelectron spectroscopy (XPS) measurements were carried on a Thermo Scientific ESCALAB 250 Xi instrument equipped with a twin-crystal microfocusing X-ray monochromator and a double-focusing full 180° spherical sector analyzer. Spectra were acquired using an Al anode (Al Kα = 1486.6 eV) operated at 72 W and a spot size of 400 μm. Survey scans were obtained at constant pass energy of 200 eV while high resolution scans were measured at a pass energy of 50 eV. The binding energy (BE) of each element was calibrated by setting the C1s line of adventitious hydrocarbon to a BE of 284.80 eV. A fitting uncertainty of 5% in the peak area was assumed and taken as the standard deviation for each concentration. Transmittance of LSC devices was obtained on a Metash UV-8000 spectrophotometer. The power conversion efficiency was evaluated using a solar cell IV test system according to a previously reported procedures.[1] Briefly, monocrystalline silicon solar cells were attached to the edge-concentrating region of LSCs, the contact portion was coupled with a fiber optics index matching gel, and the edges were sealed with black tape, and their power conversion efficiency were tested against a black background.

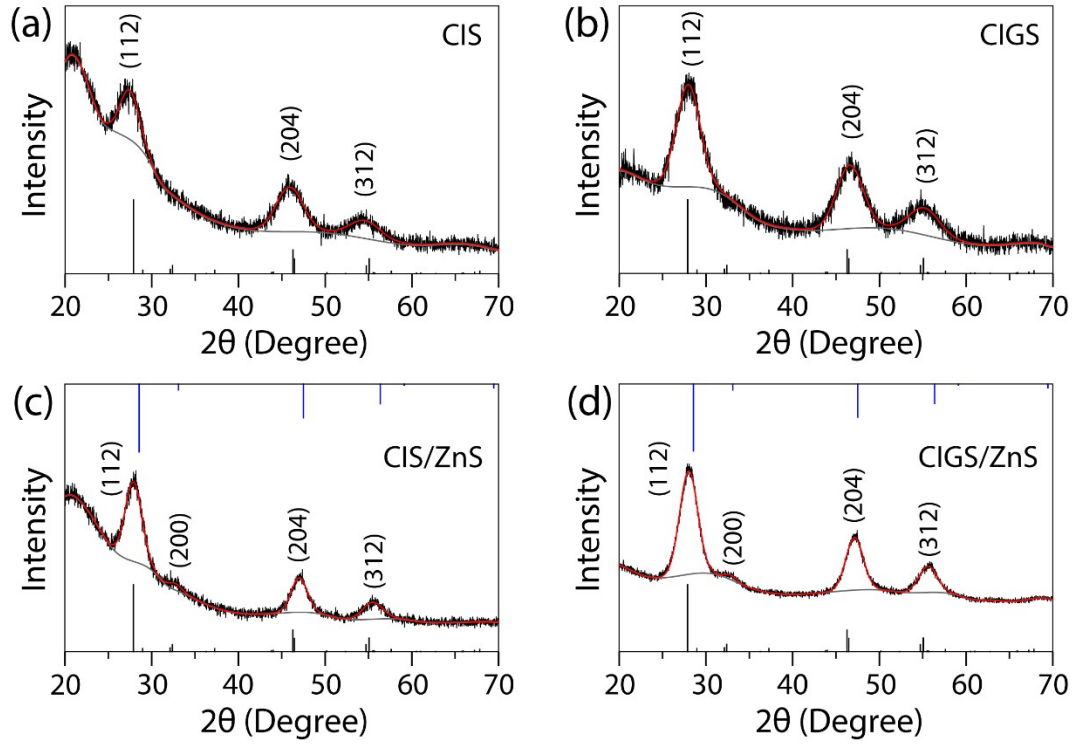

Figure S1. XRD patterns of CIS (a), CIGS (b), CIS/ZnS (c) and CIGS/ZnS (d). The sharp black lines on the bottom frame and the blue lines on the top frame represent the tetragonal chalcopyrite CIS diffraction patterns (JCPDS Card 01-085-1575) and the cubic ZnS diffraction patterns (JCPDS Card 04-008-2758), respectively. The patterns were corrected by removing background and then fitted by multi-peak Gaussian profiles. The background was modelled by an asymmetric least square smoothing fit. The multi-gaussian fits give the values of each peak integral and their full width at half maximum (FWHM), which were used to estimate the crystallite sizes based on Scherrer equation (see Table S1 shown below).

Table S1. Crystallite size, D, of CIS, CIGS, CIS/ZnS, and CIGS/ZnS QDs, are estimated from Scherrer's equation, $D = K\lambda/(\beta\cos\theta)$. K is the Scherrer constant (0.94), λ the wavelength of the X-ray source (0.15406 nm), β the full width at half maximum (FWHM) in radians, and θ the peak position in radians. The values of the peak position (θ) and FHWM (β) are determined from the fits shown in Figure S1. Crystallinity degree is calculated from the ratio of the integrated area of all crystalline peaks to the total integrated area under the XRD peaks.

CIS (Chalcopyrite)					
Plane	2θ (Degree)	β (Degree)	D (nm)	Average D (nm)	Crystallinity (%)
(112)	27.44	2.54	3.36	2.7 ± 0.5	85.2
(204)	45.89	3.59	2.51		
(312)	54.58	3.99	2.34		
CIGS (Chalcopyrite)					
Plane	2θ (Degree)	β (Degree)	D (nm)	Average D (nm)	Crystallinity (%)
(112)	27.95	3.22	2.65	2.5 ± 0.2	89.5
(204)	46.59	3.56	2.54		
(312)	55.18	4.02	2.33		
CIS/ZnS (Chalcopyrite)					
Plane	2θ (Degree)	β (Degree)	D (nm)	Average D (nm)	Crystallinity (%)
(112)	27.91	2.28	3.75	4.2 ± 0.8	93.6
(200)	32.70	1.62	5.34		
(204)	47.03	2.17	4.16		
(312)	55.49	2.65	3.54		
CIGS/ZnS (Chalcopyrite)					
Plane	2θ (Degree)	β (Degree)	D (nm)	Average D (nm)	Crystallinity (%)
(112)	28.02	2.45	3.49	4.2 ± 1.0	95.7
(200)	32.88	1.53	5.66		
(204)	47.14	2.37	3.83		
(312)	55.62	2.50	3.75		

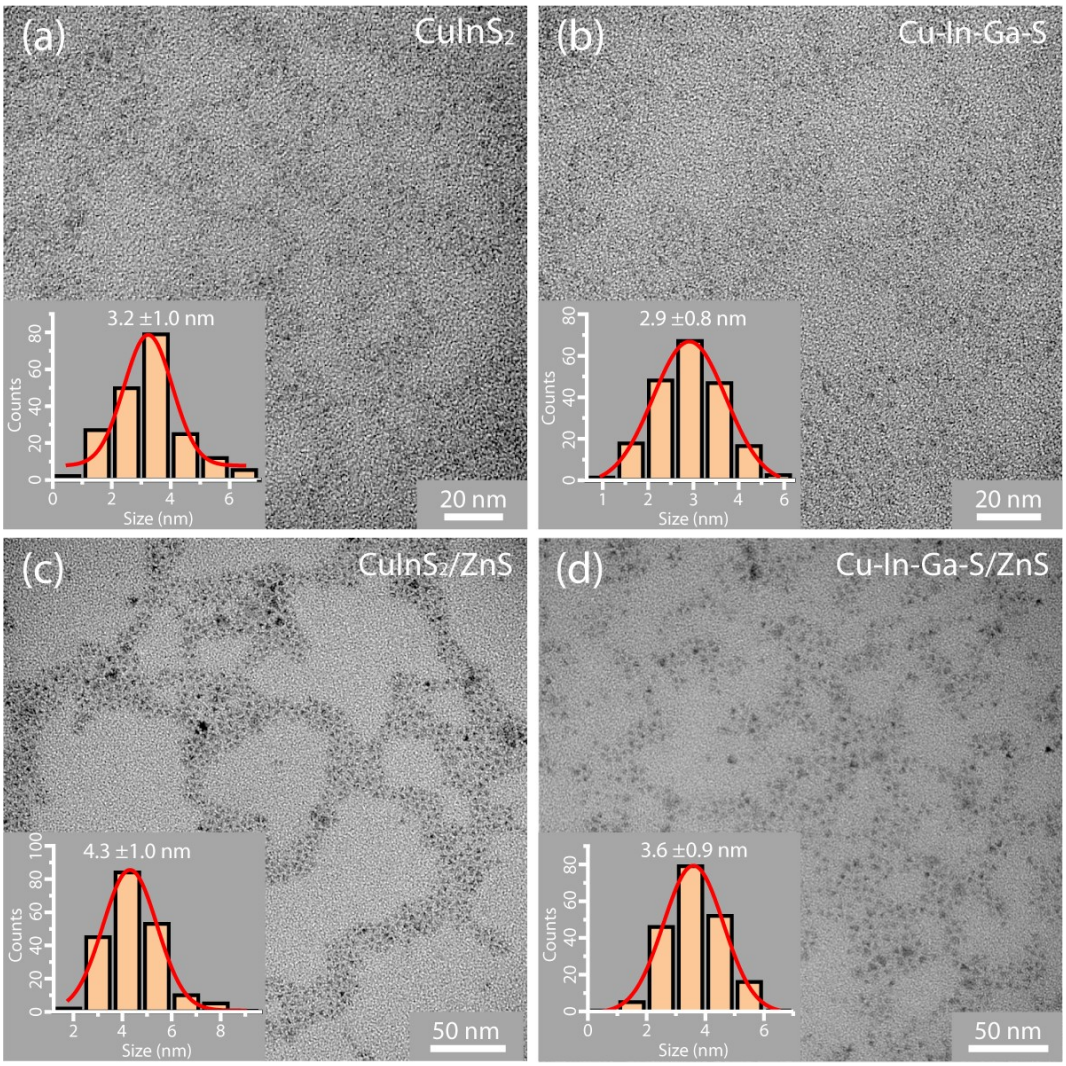

Figure S2. TEM images of CIS (a), CIGS (b), CIS/ZnS (c) and CIGS/ZnS (d). Insets in each TEM images are the size distribution histograms constructed by measuring over 200 nanoparticles and then fitted by a single Gaussian function.

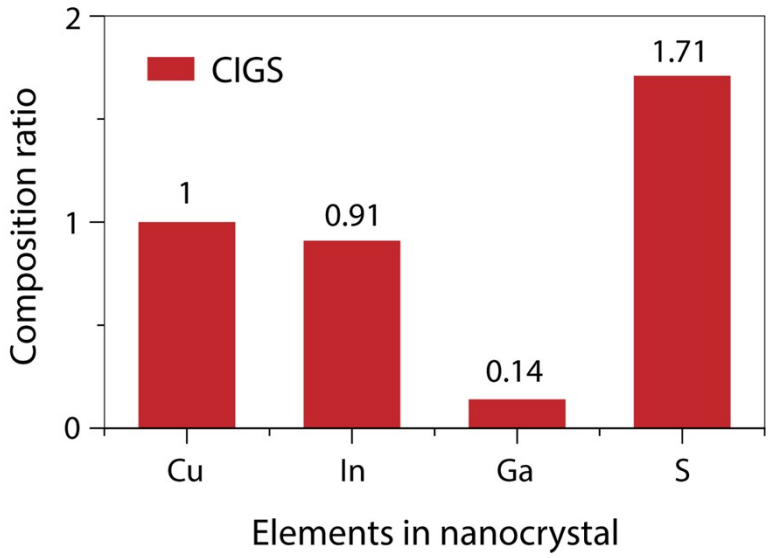

Figure S3. Relative composition of elements in CIGS QDs. The atomic ratio of each element was determined by ICP techniques, and then normalized by the ratio of Cu^{+}.

Supporting method 1: Size calculation of CIS QDs.

The average sizes of the product chalcopyrite CIS QDs were calculated according to the following equation according to the previous reported literature:[2]

$$E_g(cp\_CIS) = 1.532 + \frac{1}{0.0882d^2 + 0.587d - 0.517} \qquad \text{eq. s1}$$

where ***Eg*** is the energy (in eV) at the first absorption transition peak of chalcopyrite CIS QDs and ***d*** is the sizes. The first absorption transition energies were deduced by locating the minima of the second derivative of the absorption spectra shown in Figure S3.

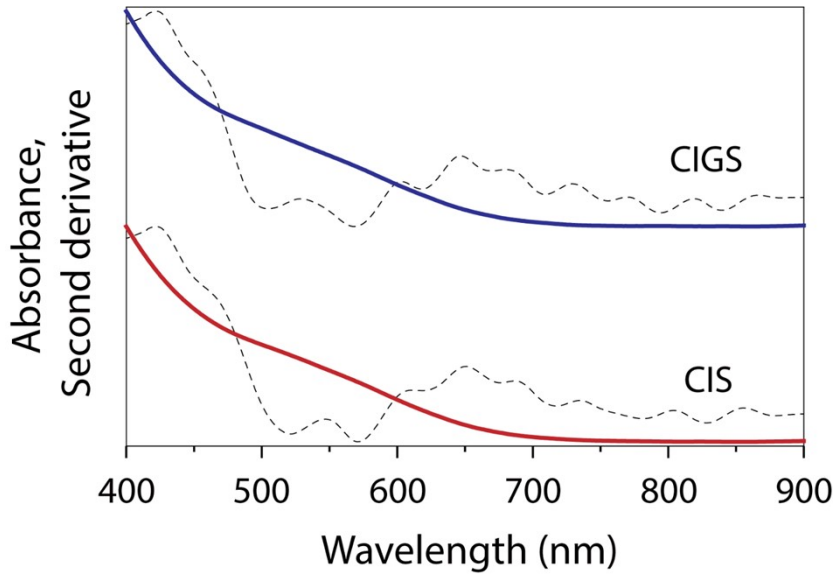

Figure S4. Absorption spectra and corresponding second derivative curves for CIS and CIGS QDs. The gray dashed curves are the second-order derivative of the corresponding absorption curves. The first absorption transition energies were then located by finding the minima of the second-order derivative curves.

Table S2. The first absorption transition energies and corresponding calculated sizes of CIS and CIGS QDs deduced from the eq. s1.

Sample	First Absorption Peak		Size (nm)
	Wavelength (nm)	Energy (eV)	
CIS	571.0	2.17	2.56
CIGS	568.0	2.18	2.53

Supporting method 2: Measurement and calculation details of PLQYs.

Samples for PLQY measurement were prepared by diluting the QDs into cyclohexane until the absorbance at excitation wavelength (442 nm) is less than 0.1 and the diluted solution was transferred into 10 mm-path-length quartz cuvettes. The integrating sphere replaced the standard sample holder inside sample chamber. The two lens assemblies that were used for the standard sample holder should be removed. Firstly, a quartz cuvette containing pure cyclohexane as a reference was placed into the integrating sphere. The reference was excited at 442 nm. In order to make sure a reflectance of 100%, the slits should be tuned until the scatter signal at 442 nm reaches the maximum sensitivity but below the detector saturation levels (e.g., excitation slit = 5; emission slit = 0.2). The emission spectrum (blue curve in Figure S1) of the reference was acquired from 430 to 800 nm. Afterwards, the as-prepared samples were measured under the same conditions (red curve).

The PLQY, η, is defined by the sum of all emitted photons, divided by the sum of all absorbed photons. The number of absorbed photons is given by the integral difference of the two scattered curves at 442 nm. The number of emitted photons can be gained by the integral difference of emission spectra. The PLQY can be calculated according the following equation,

$$\eta = \frac{E_B - E_A}{S_A - S_B}.$$

E_A and E_B denote the emission integral of the reference and the sample from 480 to 800 nm, respectively. S_A and S_B represent the scatter integral of the reference and the sample from 430 to 475 nm.

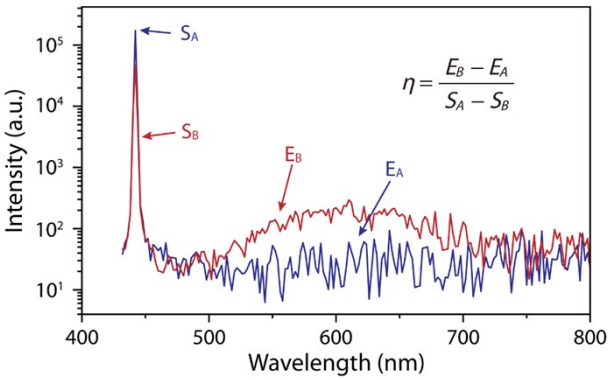

Figure S5. PL emission spectra of the reference (blue curve) and the as-prepared samples (red curve). The excitation wavelength was 442 nm and the detection wavelength was set from 430 to 800 nm. The excitation slit and emission slit were fixed at 5 and 0.2, respectively. All the measurements were conducted under the same condition.

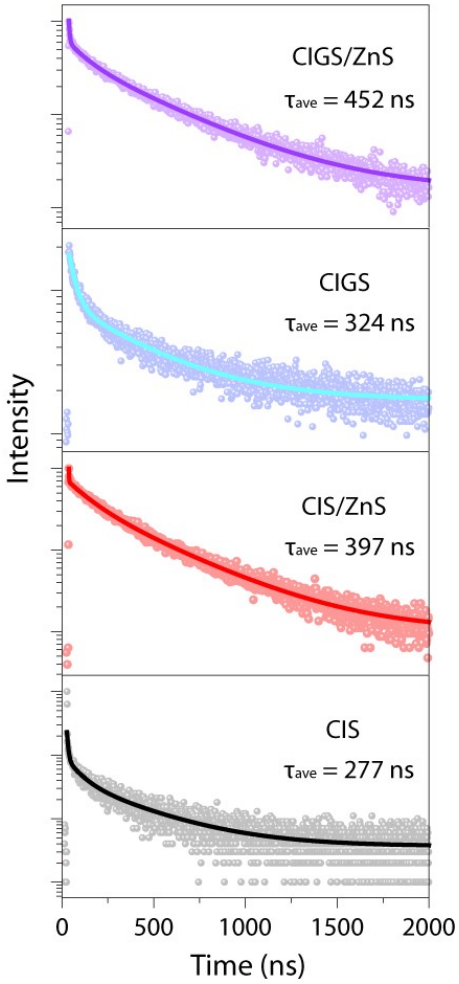

Figure S6. PL decay curves of CIS and Ga-doped CIS QDs before and after ZnS shelling.

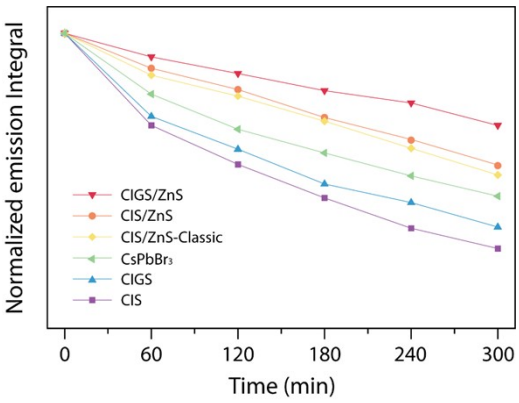

Figure S7. Photostability test of different types of QDs. The CIS, CIGS, CIS/ZnS and CIGS/ZnS QDs are the samples presented in main text Figure 2a. The CIS/ZnS-Classic QDs were prepared according to the recently reported procedures by the Chen's group.[3] The $CsPbBr_3$ nanocrystals were synthesized following the previously reported procedures by the Bramati's group.[4] All samples were diluted until the absorbance at 442 nm was equal to 0.1. The samples were continuously illuminated under an Xe lamp for 300 min with an average power of 100 mW/cm^2 under the same conditions.

Supporting method 3: Computational density functional theory (DFT).

The density functional theory (DFT) calculations were carried out with the VASP code.[5] The Perdew–Burke–Ernzerhof (PBE) functional within generalized gradient approximation (GGA)[6] was used to process the exchange–correlation, while the projectoraugmented-wave pseudopotential (PAW)[7] was applied with a kinetic energy cut-off of 500 eV, which was utilized to describe the expansion of the electronic eigenfunctions. The Brillouin-zone integration was sampled by a Γ-centered 1 × 1 × 1 Monkhorst–Pack k-point. All atomic positions were fully relaxed until energy and force reached a tolerance of 1×10^{-6} eV and 0.01 eV/Å, respectively. The dispersion corrected DFT-D method was employed to consider the long-range interactions.[8] Employing the climbing image nudged elastic band method (CI-NEB), we computed the minimum energy pathway of the reaction along with its corresponding activation barrier.

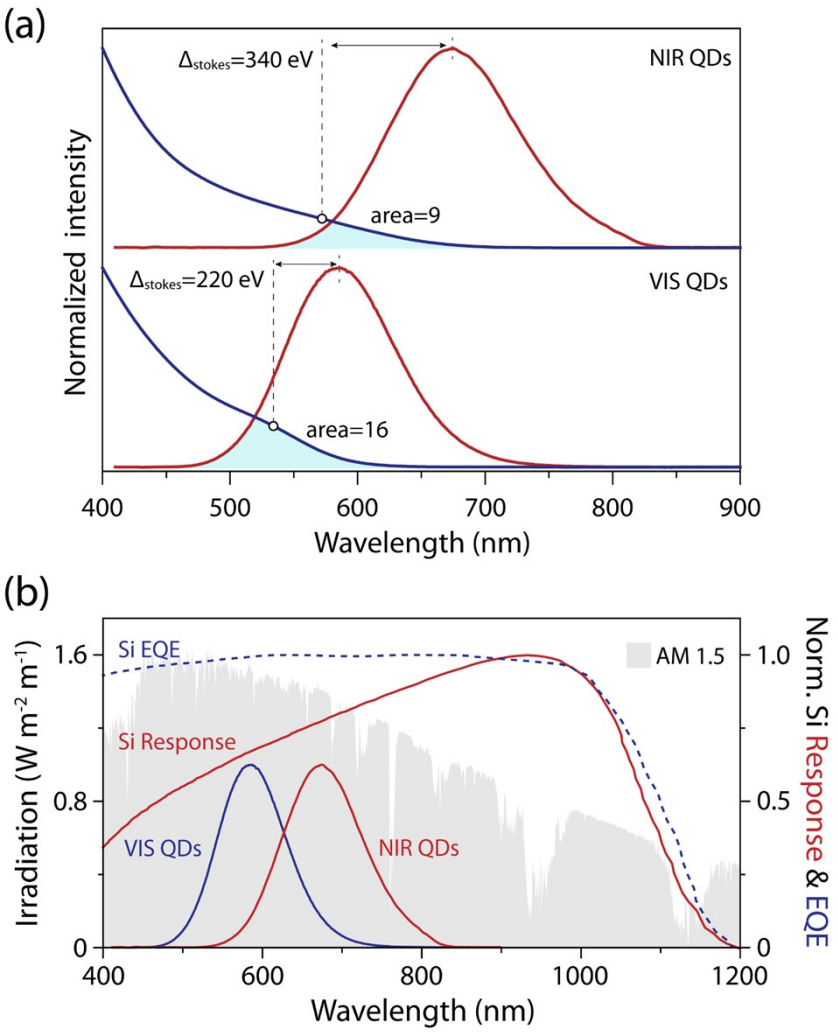

Figure S8. (a) Normalized absorption and PL spectra of VIS- and NIR-emitting CIGS/ZnS QDs synthesized by tuning the sizes of CIS cores. The cyan areas are the spectral overlap of normalized absorption and PL spectra. Δ_{stokes} denotes the Stokes shift, viz., the distance of emission peaks with respect to the first absorption transition peaks indicated by hollow circles. (b) PL spectra of VIS- and NIR-emitting CIGS/ZnS QDs, and AM 1.5 solar spectrum together with the Si response curve and external quantum efficiency curve.

Discussion: As shown in Figure S8a, the stokes shift of the NIR-emitting QDs is 1.5 times larger than that of the VIS-emitting QDs. The spectral overlap of the NIR-emitting QDs is only half of that of VIS-emitting QDs. These data confirm that NIR-emitting CIGS/ZnS QDs possess a lower re-absorption than VIS-emitting counterparts. In addition, the NIR-emitting QDs clearly show a better overlap with the response curve of the Si photovoltaic cell at the edge of the device rather than the VIS-emitting ones (Figure S8b). Therefore, the LSC devices based on NIR-emitting CIGS/ZnS QDs exhibit better performance.

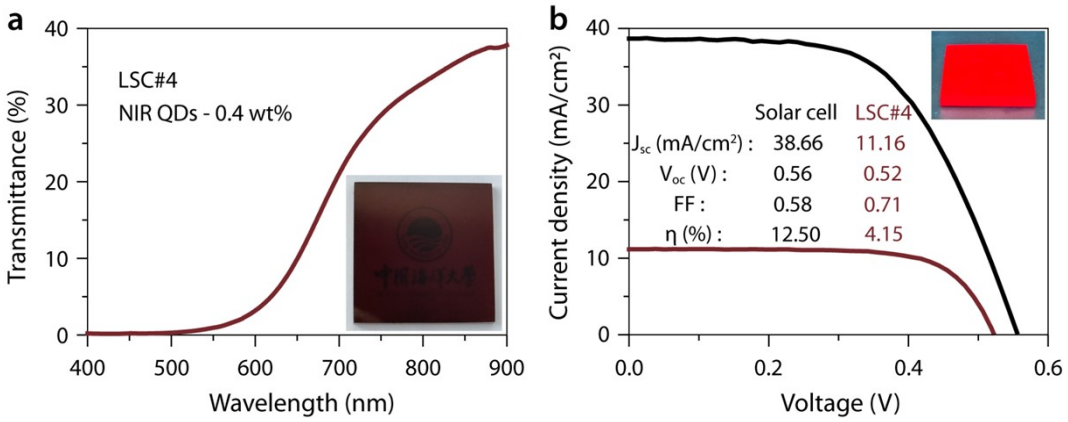

Figure S9. (a) Transmission spectra of LSCs fabricated by NIR QDs with a concentration of 0.4 wt%. Insets are the planar LSCs under ambient light. **(b)** I - V curves of the as-prepared LSC prototypes (5 × 5 × 0.5 cm) and the coupled silicon cells. They were measured with a sunlight simulator under AM1.5 illumination. Insets are the digital images of LSCs under 365 nm UV light.

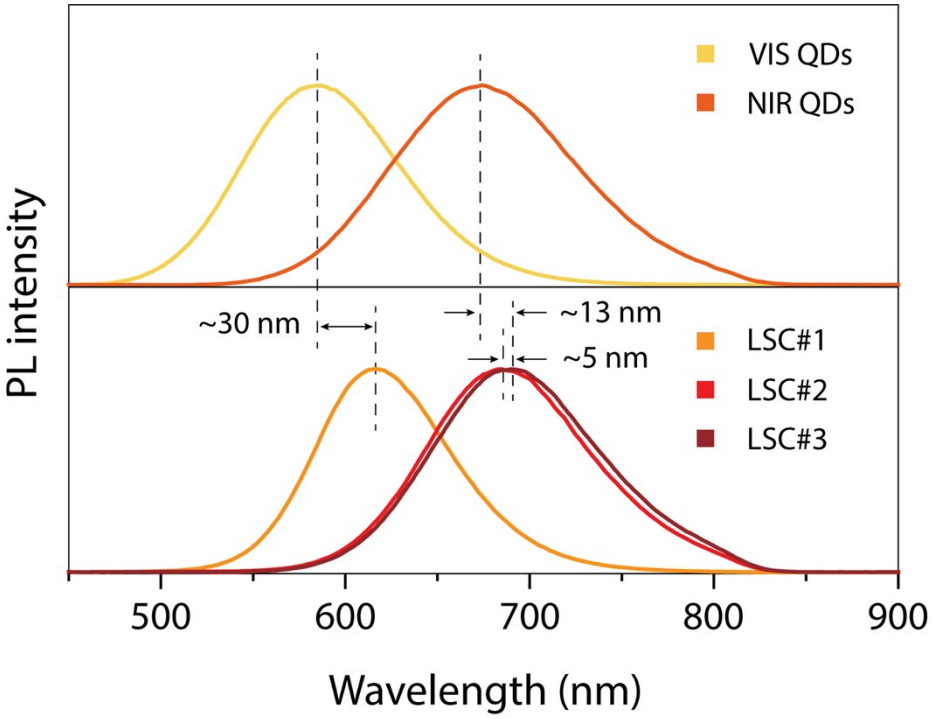

Figure S10. Comparison of PL spectra of CIGS/ZnS quantum dots in solution (top) and in LSC (bottom). The PL spectra of LSC are red-shifted compared to pure quantum dots, which may be caused by the agglomeration of quantum dots during the LSC polymerization process.

References

1. C. Yang, D. Liu and R. R. Lunt, *Joule*, 2019, **3**, 2871-2876.
2. C. Xia, W. Wu, T. Yu, X. Xie, C. van Oversteeg, H. C. Gerritsen and C. d. M. Donega, *ACS Nano*, 2018, **12**, 8350-8361.
3. Z. Liu, C. Hao, Y. Sun, J. Wang, L. Dube, M. Chen, W. Dang, J. Hu, X. Li and O. Chen, *Nano Letters*, 2024, **24**, 5342-5350.
4. M. D'Amato, L. Belzane, C. Dabard, M. Silly, G. Patriarche, Q. Glorieux, H. Le Jeannic, E. Lhuillier and A. Bramati, *Nano Letters*, 2023, **23**, 10228-10235.
5. G. Kresse, J. Furthmüller, *Computational Materials Science*, 1996, **6**, 15-50.
6. J. P. Perdew, K. Burke and M. Ernzerhof, *Physical Review Letters*, 1996, **77**, 3865-3868.
7. P. E. Blochl, *Phys Rev B Condens Matter*, 1994, **50**, 17953-17979.
8. S. Grimme, *Journal of Computational Chemistry*, 2006, **27**, 1787-1799.